NASA/TM–2015-218706

Toward a Nonlinear Acoustic Analogy: Turbulence as a Source of Sound and Nonlinear Propagation

Steven A. E. Miller
Langley Research Center, Hampton, Virginia

April 2015

NASA STI Program . . . in Profile

Since its founding, NASA has been dedicated to the advancement of aeronautics and space science. The NASA scientific and technical information (STI) program plays a key part in helping NASA maintain this important role.

The NASA STI program operates under the auspices of the Agency Chief Information Officer. It collects, organizes, provides for archiving, and disseminates NASA's STI. The NASA STI program provides access to the NTRS Registered and its public interface, the NASA Technical Reports Server, thus providing one of the largest collections of aeronautical and space science STI in the world. Results are published in both non-NASA channels and by NASA in the NASA STI Report Series, which includes the following report types:

- TECHNICAL PUBLICATION. Reports of completed research or a major significant phase of research that present the results of NASA Programs and include extensive data or theoretical analysis. Includes compilations of significant scientific and technical data and information deemed to be of continuing reference value. NASA counter-part of peer-reviewed formal professional papers but has less stringent limitations on manuscript length and extent of graphic presentations.

- TECHNICAL MEMORANDUM. Scientific and technical findings that are preliminary or of specialized interest, e.g., quick release reports, working papers, and bibliographies that contain minimal annotation. Does not contain extensive analysis.

- CONTRACTOR REPORT. Scientific and technical findings by NASA-sponsored contractors and grantees.

- CONFERENCE PUBLICATION. Collected papers from scientific and technical conferences, symposia, seminars, or other meetings sponsored or co-sponsored by NASA.

- SPECIAL PUBLICATION. Scientific, technical, or historical information from NASA programs, projects, and missions, often concerned with subjects having substantial public interest.

- TECHNICAL TRANSLATION. English-language translations of foreign scientific and technical material pertinent to NASA's mission.

Specialized services also include organizing and publishing research results, distributing specialized research announcements and feeds, providing information desk and personal search support, and enabling data exchange services.

For more information about the NASA STI program, see the following:

- Access the NASA STI program home page at http://www.sti.nasa.gov

- E-mail your question to help@sti.nasa.gov

- Phone the NASA STI Information Desk at 757-864-9658

- Write to:
  NASA STI Information Desk
  Mail Stop 148
  NASA Langley Research Center
  Hampton, VA 23681-2199

NASA/TM–2015-218706

Toward a Nonlinear Acoustic Analogy: Turbulence as Source of Sound and Nonlinear Propagation

Steven A. E. Miller
Langley Research Center, Hampton, Virginia

National Aeronautics and
Space Administration

Langley Research Center
Hampton, Virginia 23681-2199

April 2015

Acknowledgments

The author is grateful for continuous support from the National Aeronautics and Space Administration (NASA), Advanced Air Vehicles Program, Commercial Supersonic Technology Project. Brian Howerton of NASA Langley Research Center provided measurements from the NASA Langley Liner Lab Normal Incidence Tube. Emily Mazur, a 2012 NASA Langley Aerospace Research Student Scholars Program participant, is acknowledged for evaluating numerically the Blackstock bridging function.

Available from:

NASA STI Program / Mail Stop 148
NASA Langley Research Center
Hampton, VA 23681-2199
Fax: 757-864-6500

Abstract

An acoustic analogy is proposed that directly includes nonlinear propagation effects. We examine the Lighthill acoustic analogy and replace the Green's function of the wave equation with numerical solutions of the generalized Burgers' equation. This is justified mathematically by using similar arguments that are the basis of the solution of the Lighthill acoustic analogy. This approach is superior to alternatives because propagation is accounted for directly from the source to the far-field observer instead of from an arbitrary intermediate point. Validation of a numerical solver for the generalized Burgers' equation is performed by comparing solutions with the Blackstock bridging function and measurement data. Most importantly, the mathematical relationship between the Navier-Stokes equations, the acoustic analogy that describes the source, and canonical nonlinear propagation equations is shown. Example predictions are presented for nonlinear propagation of jet mixing noise at the sideline angle.

Nomenclature

Symbols

$\boldsymbol{A}$	Arbitrary vector quantity
A_{ijlm}	Coefficient matrix
A_{ij}	Subset of A_{ijlm}
B_n	Fourier coefficients of BBF
c	Speed of sound
D	Nozzle exit diameter
D_j	Fully expanded diameter
e_o	Total energy
F	Fourier series dependent on x
g	Arbitrary function or Green's function
J_n	Bessel function of the first kind of order n
j	Integer index
K	Fourier coefficient
k	Wavenumber
k_{max}	Maximum turbulent kinetic energy within jet plume
l	Turbulent length scale
M	Mach number
M_a	Acoustic Mach number
M_c	Convective Mach number constant
M_d	Design Mach number
M_j	Fully expanded Mach number
m	Integer index
P_f	Scaling constant for spectral density
Pr	Prandtl number
p	Pressure
$\boldsymbol{q}$	Heat-flux
$\tilde{q}$	Square of $\tilde{p}$
R	Gas constant or propagation distance
R_{ijlm}	Two-point cross-correlation of Lighthill stress tensor
$\boldsymbol{r}$	Vector from source to observer
r	Radial coordinate
S	Spectral density
St	Strouhal number
S_y	Equivalent source strength per unit length
T	Thermodynamic temperature
T_d	Thermal diffusion rate
T_{ij}	Lighthill stress tensor
t	Time
$\boldsymbol{u}$	Velocity
$\boldsymbol{x}$	Observer or position
$\boldsymbol{y}$	Source position or particle displacement
y_c	Jet potential core length
α	Atmospheric absorption coefficient
β	Coefficient of nonlinearity or dispersion coefficient
β_s	A constant within the two-point cross-correlation
Γ	Group of coefficients involving nonlinearity
γ	Ratio of specific heats
δ	Dirac delta function or viscous terms
δ_{ij}	Kronecker delta function
ϵ	$\beta(\rho_\infty c_\infty^3)^{-1}$
$\boldsymbol{\eta}(\xi,\eta,\zeta)$	Source separation vector
μ	Kinematic viscosity
ν	Dynamic viscosity
ξ	Momentum in Lagrangian coordinates or source separation in x direction
ρ	Density
σ	Shock formation distance or amplification factor
τ	Retarded time
τ_s	Turbulent time scale
τ_{ij}	Viscous stress tensor
Φ_{sh}	Earnshaw phase angle
ϕ	Arbitrary vector quantity or wave emission time
ω	Radial frequency

Abbreviations

BBF	Blackstock bridging function
NIT	Normal Incidence Tube
PSD	Power spectral density
SPL	Sound pressure level
TTR	Total temperature ratio

1 Introduction

The physical mechanism and associated mathematical model to predict acoustic radiation from high speed compressible fluid turbulence continues to elude investigators after decades of research. In most fluid flows, the intensity of turbulence gives rise to acoustic radiation that propagates according to the theory of linear acoustics and dissipative effects dominate nonlinear effects. When turbulence is highly intense the resultant acoustic waves have magnitudes that result in nonlinear propagation due to dominance of nonlinear terms over dissipative terms contained in the equations of motion. The radiating waves contain all non-zero frequency components, are very energetic, and coalesce into many discontinuities (shock waves). Here, we seek a unified theory of the radiation source using an acoustic analogy combined with the nonlinear propagation effects approximately governed by the generalized Burgers' equation.

High intensity compressible turbulence is present within the exhaust flow created by rocket and high performance air breathing jet engines. The acoustic radiation created by these exhaust flows is potentially harmful to the flight vehicle airframe, launchpad, or flight deck through the mechanism of sonic fatigue or sonic failure. It is also potentially harmful or annoying to the surrounding community and natural environment. A few recent investigations (among many conducted over decades) illustrate the relevance of this contemporary problem via the noise produced by aircraft. Recently, Neilsen et al. [1] conducted measurements of the 'F-22A Raptor' flight vehicle with afterburning engines. They examined the spectral characteristics spatially and the waveforms' nonlinear indicators as described by Gee et al. [2], and showed that nonlinear propagation effects are important. Though many nonlinear indicators have been proposed, Gee et al. [2] created two that are complimentary to traditional spectral measurement approaches, and successfully separated geometric acoustic effects from nonlinear propagation effects. Petitjean et al. [3] performed experiments to examine nonlinear distortion of acoustic waves and waveforms in the time and frequency domains. They proposed that the convective Mach number of turbulent structures is highly correlated with nonlinear effects, which is certainly the case for high speed rocket and jet exhaust. Highly energetic jet noise spectra were recently analyzed by Tam and Parrish [4], and they proposed that the divergence of measurements from relatively low intensity similarity spectra might be due to indirect combustion noise from the afterburner. The peak intensities calculated by Tam and Parrish [4] are 178 dB. Morfey and Howell [5] conducted flight tests and showed that the inclusion of finite-amplitude noise propagation theory must be used to account for observed aircraft flyover effects. Thus, prediction approaches for jet noise created by the F-22 or similar aircraft must account for nonlinear propagation effects.

Contemporary studies of rocket noise with emphasis on nonlinear propagation have recently been conducted. Rocket noise data was analyzed by McInerny and Olcmen [6], and they observed many shocks within the waveforms at all angles and distances from the flight vehicle. They concluded that nonlinear effects must be accounted for to explain the many discontinuities observed in the measured waveform. Recently, Gee et al. [7] characterized the rocket noise source by performing measurements of a statically fired rocket engine. These measurements yielded insight into the rocket noise source strength and spatial distribution based upon near-field microphone measurement. Nonlinear indicators from these measurements implied that the source is intense and necessitates the use of finite-amplitude acoustic theory for sound propagation. In these investigations, the far-field noise can only be obtained by propagating the measured signal from the near-field to the far-field. These contemporary investigations (and those in the past) measure the far-field noise directly or propagate the measured near-field signal to the far-field from an intermediate point. Here, we attempt to create a prediction method to propagate acoustic radiation from high intensity jets to the far-field directly from the source.

In this paper, the Navier-Stokes equations are used to derive the generalized Burgers' equation and the Lighthill [8] acoustic analogy. The form of the acoustic analogy and associated sources are modeled for jet mixing noise using the approach described by Miller [9]. We retain the Green's function of the wave equation as an argument for the spectral density in the far-field. It is argued that the modulus squared of the Green's function of the wave equation, contained explicitly in the acoustic analogy, can be approximated with solutions of the generalized Burgers' equation. For low intensity turbulence, limiting forms of solutions of the generalized Burgers' equation are equal to those of the wave equation. When the radiation source is relatively more intense, then nonlinear effects present within the generalized Burgers' equation are captured directly within the acoustic analogy approach. The combination of approximating the Green's function of the wave equation with the generalized Burgers' equation leads to a unique approach that overcomes limitations of previous linear acoustics approaches. However, some important assumptions must be made. In particular, for propagation purposes only, the source origin is approximated at a point in space. The source spectrum is still evaluated with a volumetric integral.

This paper first surveys the mathematical theory of the governing equations of motion and the subsequent derivation of the source model and propagation model. Particular solutions of propagation models are developed. The relationship between the source model and the propagation model is shown. The process of evaluating the closed form models numerically is discussed. Next, example calculations are presented that illustrate the physics of nonlinear propagation for both the limiting cases and the model, and are compared with select measurement data. Finally, predictions are conducted for the power spectral density of high intensity jet mixing noise at various observer positions to illustrate the effect of nonlinear propagation.

2 Mathematical Theory

This section is heavily based upon the work of Schlicting and Gersten [10], Crighton [11], and Blackstock [12, 13]. The equations of motion are introduced, a source model and propagation model are derived independently, and their connection is shown. We begin with the Navier-Stokes equations as shown by Schlicting and Gersten [10] where the continuity equation is

$$\frac{\partial \rho}{\partial t} + \frac{\partial \rho u_i}{\partial x_i} = 0, \tag{1}$$

the momentum equation is

$$\frac{\partial \rho u_i}{\partial t} + \frac{\partial \rho u_i u_j}{\partial x_j} = \frac{\partial \tau_{ij}}{\partial x_j}, \tag{2}$$

and the energy equation is

$$\frac{\partial \rho e_o}{\partial t} + \frac{\partial \rho u_j e_o}{\partial x_j} = -\frac{\partial u_j p}{\partial x_j} - \frac{\partial q_j}{\partial x_j} + \frac{\partial u_i \tau_{ij}}{\partial x_j}, \tag{3}$$

where

$$\tau_{ij} = -p\delta_{ij} + \mu\left(\frac{\partial u_i}{\partial x_j} + \frac{\partial u_j}{\partial x_i}\right) - \frac{2}{3}\mu\frac{\partial u_k}{\partial x_k}\delta_{ij}, \tag{4}$$

e_o is the total energy, p is the pressure, t is time, $\boldsymbol{u}$ is the velocity vector, $\boldsymbol{q}$ is the heat-flux, $\boldsymbol{x}$ is the spatially independent variable, δ_{ij} is the Kronecker delta function, ρ is the density, and μ is the viscosity. We assume that the gas is ideal and $p = \rho RT$, where R is the gas constant and T is the temperature.

2.1 The Propagation of Weakly Nonlinear Waves

We simplify the Navier-Stokes equations by assuming that $\boldsymbol{u} = \nabla\phi + \nabla \times A$, where ϕ and A are used to represent the dependent variable u. Only the first- (linear), second-order (nonlinear), and dissipative terms that are linear relative to dependent variables and diffusion coefficients are retained. We also assume that the diffraction coefficients are constant and equal to their reference (ambient) values. The Prandtl number is $Pr = \nu T_d^{-1}$, where the kinematic viscosity is $\nu = \mu\rho_\infty^{-1}$ and T_d is the thermal diffusion rate. We obtain

$$\begin{aligned} -c_\infty^2 \nu Pr^{-1}\nabla^4\phi + \left(2 + \frac{\mu_v}{\mu} + \frac{\gamma}{Pr}\right)\nu\nabla^2\frac{\partial^2\phi}{\partial t^2} + \frac{\partial}{\partial t}\left(c_\infty^2\nabla^2\phi - \frac{\partial^2\phi}{\partial t^2}\right) \\ = \frac{\partial}{\partial t}\left[2\nabla\phi\cdot\nabla\frac{\partial\phi}{\partial t} + (\gamma-1)\frac{\partial\phi}{\partial t}\nabla^2\phi\right] \end{aligned} \tag{5}$$

and

$$\frac{\partial \boldsymbol{A}}{\partial t} + \nu\nabla\times\nabla\times\boldsymbol{A} = 0, \tag{6}$$

where sub v signifies the dilatational viscosity. If we let $\boldsymbol{A}$ be a constant (the flow is irrotational) and allow the temperature boundary condition of the fluid domain to vary, we find a simplified form

$$c_\infty^2\nabla^2\phi - \frac{\partial^2\phi}{\partial t^2} + \left[2 + \frac{\mu_v}{\mu} + \frac{\gamma-1}{Pr}\right]\nu\nabla^2\frac{\partial\phi}{\partial t} = 2\nabla\frac{\partial\phi}{\partial t}\cdot\nabla\phi + (\gamma-1)\frac{\partial\phi}{\partial t}\nabla^2\phi. \tag{7}$$

Equation 7 is the basis for a wide range of nonlinear propagation investigations and can be used to accurately predict 'weakly' nonlinear propagation of waves.

Using Eqn. 7 we seek to derive the generalized Burgers' equation. We assume that the flow has the properties of a set of symmetries. These symmetries are cylindrical, spherical, and planar. Also, we assume that $k_\infty r >> 1$, where $k_\infty = \omega c_\infty^{-1}$ is the 'linear' wavenumber, ω is the radial frequency, and c_∞ is the ambient speed of sound. Using these assumptions Eqn. 7 simplifies to

$$\frac{\partial u}{\partial t} + c_\infty\frac{\partial u}{\partial r} + \frac{\gamma+1}{2}u\frac{\partial u}{\partial r} + \frac{jc_\infty u}{2r} = \frac{\delta}{2}\frac{\partial^2 u}{\partial r^2}, \tag{8}$$

where $j = 0$, 1 or 2 for plane, cylindrical, or spherically symmetric (outgoing waves) solutions respectively and δ is a group of viscous terms. Crighton [11] wrote this 'generalized Burgers' equation' non-dimensionally and compactly as

$$\frac{\partial W}{\partial Z} - W\frac{\partial W}{\partial\Theta} = \frac{\delta\omega}{2c_\infty^2}g(Z)\frac{\partial^2 W}{\partial\Theta^2}, \tag{9}$$

where for $j = 0$, $W = U$, $Z = R$, and $g(Z) = 1$, for $j = 1$, $W = R^{1/2}U$ and $Z = 2R^{1/2}$, and $g(Z) = Z/2$, and for $j = 2$, $W = RU$, $Z = \ln R$, and $g(Z) = \exp[Z]$. Here, $U = (\gamma+1)u(2c_\infty)^{-1}$, $R = k_\infty r$, $\Theta = \omega\tau$, and τ is the retarded time. Unfortunately, the general solution of Eqn. 8 is unknown, let alone a proof of a solution's existence. Recently some *exciting* exact bi-soliton solutions have been proposed by Vladimirov and Maczka [14]. Crighton [11] summarizes some specific earlier solutions of Eqn. 9. Let us temporarily focus our attention on solutions with planar symmetry where the wave fronts are perpendicular to the x direction. We write Eqn. 7 or 8, after integration with respect to time and differentiation with respect to x as

$$\frac{\partial u}{\partial t} + \left(c_\infty + \frac{\gamma + 1}{2} u \right) \frac{\partial u}{\partial x} = \frac{1}{2} \delta \frac{\partial^2 u}{\partial x^2}. \tag{10}$$

This equation can be written in a more compact form by making a coordinate transform from x to $x - c_\infty t$. Also, for reasons that will become apparent later, we are interested in solutions of the generalized Burgers' equation cast as a boundary value problem, that is a solution where at some point in space the pressure is defined as a function of time. The waveform evolves from this initial point in the direction of propagation. We also assume $c_\infty \phi_x \approx -\phi_t$, the retarded time is $\tau = t - x c_\infty^{-1}$, and subsequently obtain an equation shown by Mendousse [15]. We write the resultant equation of Mendousse [15] as a pressure perturbation using the relation $p \approx \rho_\infty c_\infty u$ and find

$$\frac{\partial p}{\partial x} - \epsilon p \frac{\partial p}{\partial \tau} = \frac{\delta}{2 c_\infty^3} \frac{\partial^2 p}{\partial \tau^2}, \tag{11}$$

where $\beta = (\gamma + 1)/2$ is the coefficient of nonlinearity, $\epsilon = \beta / \rho_\infty c_\infty^3$, and

$$\delta = \nu \left(\frac{4}{3} + \frac{\mu_v}{\mu} + (\gamma - 1) \, Pr^{-1} \right). \tag{12}$$

Similar processes can be used to find equations for spherically and cylindrically symmetric outgoing waves. These can be written in a general form as (containing an extra term relative to Eqn. 11)

$$\frac{\partial p}{\partial x} + m \frac{p}{r} - \epsilon p \frac{\partial p}{\partial \tau} = \frac{\delta}{2 c_\infty^3} \frac{\partial^2 p}{\partial \tau^2}, \tag{13}$$

where $m = 0$, $1/2$, and 1 for plane, cylindrical, and spherical waves, respectively. Equation 13 can be found more rigorously as shown by Lighthill [16]. Saxena et al. [17] wrote Eqn. 13 in a form more amenable to numerical solution in the frequency domain

$$\frac{\partial \tilde{p}}{\partial r} + m \frac{\tilde{p}}{r} + (\alpha + i\beta) \, \tilde{p} = \frac{i \omega \epsilon}{2} \tilde{q}, \tag{14}$$

where $\tilde{q} = \tilde{p}^2$, α is the atmospheric absorption coefficient, and β is the dispersion coefficient. The tilde represents a Fourier transform. In certain circumstances Eqn. 13 can be solved analytically for carefully chosen boundary conditions, and a subset of these solutions are described in the next sections. In most cases of practical interest, Eqn. 13 must be solved numerically. The boundary condition is typically based on a broadband pressure time history or spectrum. The boundary condition is assumed to be periodic, and its connection with the source model will be discussed in the next section.

We survey a numerical method for the solution of Eqn. 13. The approach is heavily based upon the methods developed by Lee et al. [18] and Saxena [19]. First, the Fourier transform and square of the Fourier transform of a pressure time history are calculated (boundary condition). It is assumed that the pressure time history (derived from a 'source spectrum' with random phase) is periodic in time. An explicit second order Runge-Kutta spatial marching technique is used to propagate the waveform in the radiation direction. The real and imaginary parts of $\tilde{p}$ and $\tilde{q}$ are advanced in space at each discrete step. After each spatial step marched, a filter window is applied to remove numerical noise, and the complex atmospheric absorption and dispersion as a function of frequency are applied. Also, a Lanczos filter as described by Duchon [20] is applied at each spatial step to help minimize the Gibbs phenomenon. The complex coefficients of atmospheric absorption and

dispersion are calculated using the method of Bass et al. [21, 22]. When the waveform integration reaches the observer, the inverse Fourier transform of $\tilde{p}$ is performed to recover the pressure time history.

2.2 The Fay Solution

We now examine certain limited solutions for finite-amplitude wave propagation. Fay [23] derived an equation of motion using physical arguments for the perturbation of a gas in a single spacial dimension and time. It can easily be shown that the equation of motion that Fay [23] considered is based upon Eqn. 2 with certain assumptions. These assumptions include the flow varying in one spatial dimension, varying in time, the dependent variables are small in fluctuation, that fluctuations in $u >> \rho$, viscosity is a constant, and additionally that the boundary condition of temperature is fluctuating. Fay did not explicitly use an assumption regarding temperature fluctuations at the boundary, but it is required here to obtain Fay's governing equation from the Navier-Stokes equations. Multiplying the resultant equation by a differential dx to give a volume per unit length x, yields Fay's governing equation

$$\rho_\infty \frac{\partial u}{\partial t} dx = -\frac{\partial p}{\partial x} dx + \frac{4}{3}\mu \frac{\partial^2 u}{\partial x^2} dx. \tag{15}$$

Fay [23] assumes that compression is adiabatic

$$\frac{p}{p_\infty} = \left(\frac{\rho}{\rho_\infty}\right)^\gamma, \tag{16}$$

which implies for the one-dimensional problem

$$\frac{p}{p_\infty} + 1 = \left(\frac{\partial y}{\partial x}\right)^{-\gamma}, \tag{17}$$

where y is the distance of a particle from a 'resting plane' of reference at time t. Assuming that $c_\infty^2 = \gamma p_\infty \rho_\infty^{-1}$, Fay focuses on a solution of the resulting equation

$$c_\infty^2 \frac{\partial^2 y}{\partial x^2} = \frac{\partial y}{\partial x}^{\gamma+1} \left[\frac{\partial^2 y}{\partial t^2} - \frac{4\mu}{3\rho_\infty}\frac{\partial}{\partial t}\left(\frac{\partial^2 y}{\partial x^2}\right)\right]. \tag{18}$$

Fay [23] assumes that the solution is periodic and $y = x + F$, where F is a Fourier series with coefficients that are dependent on x. After substituting the relation between y and F into Eqn. 18 and assuming that $\partial F/\partial x$ can be represented as a Fourier series, Fay finds the solution for $\partial F/\partial x$ and its Fourier coefficients. The solution of Eqn. 18 in terms of $\partial F/\partial x$ is

$$\begin{aligned} \frac{\partial F}{\partial x} &= \log\left[\frac{16\mu\omega}{3\rho_\infty(\gamma+1)c_\infty^2 K_{1,1}}\right] \\ &- \frac{8\mu\omega}{c_\infty^2\rho_\infty\left(\gamma+1\right)} \sum_{n=1}^{n=\infty} \frac{\sin n\left(\omega t - \omega x/c_\infty\right)}{\sinh n\left[\log\left[\frac{16\mu\omega}{3c_\infty^2\rho_\infty(\gamma+1)K_{1,1}}\right] + \frac{2x\mu\omega^2}{3\rho_\infty c_\infty^3}\right]} \end{aligned} \tag{19}$$

where $K_{1,1}$ is an arbitrary coefficient that can be set to match a periodic boundary condition. Note that $\partial F/\partial x$ is the ratio of the change in volume relative to specific volume in the undisturbed medium, thus

$$p = p_\infty\left[\left(\frac{\partial y}{\partial x}\right)^{-\gamma} - 1\right] = -p_\infty\gamma\left[\frac{\partial F}{\partial x} - \left(\frac{\gamma+1}{2!}\right)\left(\frac{\partial F}{\partial x}\right)^2 + ...\right]. \tag{20}$$

Using this relation and Eqn. 19 yields

$$\frac{p}{p_\infty} = \frac{32}{3}\frac{\mu\omega}{c_\infty^2\rho_\infty}\left(\frac{\gamma}{\gamma+1}\right)\sum_{n=1}^{n=\infty}\frac{\sin n\left(\omega t - \omega x/c_\infty\right)}{\sinh n\left[\log\left[\frac{16\mu\omega}{3\rho_\infty(\gamma+1)c_\infty^2 K_{1,1}}\right] + \frac{2x\mu\omega^2}{3c_\infty^3\rho_\infty}\right]}. \tag{21}$$

Equation 21 represents the Fay [23] solution of Eqn. 15 that is derived after many simplifications from the Navier-Stokes equations. Blackstock [24] writes Eqn. 21 in a simplified form

$$\frac{p}{p_\infty} = \sum_{n=1}^{n=\infty}\frac{2\Gamma^{-1}}{\sinh\left[n(1+\sigma)\Gamma^{-1}\right]}\sin n(\omega t - kx), \tag{22}$$

where Γ groups the coefficients involving nonlinearity relative to dissipation and σ is the non-dimensional propagation distance normalized by the shock pressure

$$\sigma = \frac{x}{\overline{x}} = \frac{p_\infty\beta kx}{\rho_\infty c_\infty^2}. \tag{23}$$

2.3 The Fubini Solution

Another limited solution for finite-amplitude wave propagation is now presented that was proposed by Fubini [25]. It was brought to the attention of the larger acoustic community through the work of Westervelt [26]. Fubini used a unique approach and sought a solution of the non-conservative one-dimensional momentum equation without viscous effects in Lagrangian form

$$\frac{\partial^2\xi}{\partial t^2} + \frac{\partial\xi}{\partial t}\frac{\partial^2\xi}{\partial x\partial t} = -\frac{1}{\rho}\frac{\partial p}{\partial x}, \tag{24}$$

where a is a function of x only and $x = a + \xi$. Here, ξ is the displacement of the particle at position a at time t. The problem is solved with the boundary condition $u(0,t) = u_o\sin[\omega t]$. The solution approach is straightforward, and Fubini [25] used the approach of Earnshaw [27] and wrote a closed-form solution for u as a binomial series. After retaining the first two terms of the binomial series the solution of Eqn. 24 is

$$u(x,t) = u_o\sin\left[\omega t - \frac{\omega x}{c_\infty}\left(1 - \beta u c_\infty^{-1}\right)\right], \tag{25}$$

where $\beta = \omega u_\infty(c_\infty^2 M_a k)^{-1}$ and M_a is the acoustic Mach number. It is desirable to change the form of Eqn. 25 to something more convenient for our purposes. The term uu_∞^{-1} is expanded as a series

$$\frac{u}{u_\infty} = \sum_{n=1}^{\infty} B_n\sin n(\omega t - kx), \tag{26}$$

where

$$B_n = \frac{1}{n}\int_0^{2\pi}\frac{u}{u_\infty}\sin[n(\omega t - kx)]d(\omega t - kx). \tag{27}$$

Using conservation of momentum in an Eulerian framework, Fubini [25] showed a simplified form

$$B_n = \frac{2}{n\sigma}J_n\left[n\sigma\right], \tag{28}$$

where J_n are the Bessel functions of the first kind of order n. Using the relation $p = \rho_\infty c_\infty u$ and combining Eqn. 26 and 28, the solution can be written

$$\frac{p}{p_\infty} = \sum_{n=1}^{\infty} \frac{2}{n\sigma} J_n[n\sigma] \sin n\left(\omega t - kx\right) \tag{29}$$

that is also shown by Blackstock [24]. The solutions for weakly nonlinear planar wave propagation of Fay [23] and Fubini [25] (Eqns. 21 and 29) are very different because they are particular solutions of the Navier-Stokes equations given greatly different assumptions. In the next section Blackstock [24] reconciles these differences.

2.4 The Blackstock Bridging Function

Blackstock [24] examined the solutions of Fay [23] and Fubini [25] in an attempt to reconcile their differences. The Fay and Fubini solutions are not accurate in a range of $\sigma = 1$ to $\sigma \approx 3.5$, that is the transition region from the continuous solution to a discontinuous solution. Blackstock [24] 'bridged this gap' between the two solutions by using 'weak shock theory,' where progressive wave relations are used to describe continuous sections of the waveform between shocks (discontinuities in the solution). Unlike other attempts to find more general solutions, the approach does not directly make use of the generalized Burgers' equation or its variations. Using weak shock theory the governing equations are

$$u = g(\phi), \tag{30}$$

where u is the particle velocity, g is a function, and ϕ represents the wave emission time. An equation is created that relates the difference of wave emission time with source time

$$\tau = \phi - (\beta c_\infty^{-2}) g(\phi). \tag{31}$$

The system of equations is closed by defining an equation that governs the wave path and amplitude of each shock wave

$$\frac{dt_s'}{dx} = -\frac{1}{2}\beta c_\infty^{-2}(u_a + u_b), \tag{32}$$

where subscripts a and b represent quantities just preceding and following the shock front and a prime denotes evaluation at the retarded time. Equations 30 through 32 are a system of equations based on weak shock theory, and these equations are solved directly for u after eliminating ϕ by substitution. Like Fay [23] and Fubini [25], the solution is sought as a boundary value problem by specifying $u(0,t) = u_o \sin[\omega t]$ for $t >> 0$. A transcendental equation for the shock amplitude results, and the solution process follows that of Fubini almost exactly as shown in the previous section, where a Fourier series is proposed. After many straightforward mathematical operations are performed as shown by Blackstock [24], an expression for p is obtained

$$p(x,t) = p_o \sum_{n=1}^{\infty} B_n \sin\left[n\omega\tau\right], \tag{33}$$

where p_o represents the initial wave amplitude at $x = 0$. Equation 33 is the Blackstock bridging function (BBF). The coefficients B_n are

$$B_n = \frac{2}{n(1+\sigma)} + \frac{2}{n\pi\sigma} \int_{\Phi_{sh}}^{\pi} \cos\left[n\left(\Phi - \sigma \sin\Phi\right)\right] d\Phi, \tag{34}$$

where n is the harmonic number and Φ_{sh} is the Earnshaw phase variable. Coefficients B_n are evaluated with a numerical integration technique. Here, Φ_{sh} satisfies

$$\Phi_{sh} = \sigma \sin\Phi_{sh} \tag{35}$$

and is transcendental. Generally it must be evaluated numerically.

2.5 Acoustic Radiation Source Modeling using the Acoustic Analogy

We have now obtained a general equation for the propagation of weakly nonlinear acoustic radiation (Eqn. 13) and a highly accurate analytical solution (Eqn. 33) to validate more general numerical solutions. Here, we seek to predict the broadband source spectrum for use with the developed propagation theory using the same set of governing equations. We apply the partial derivative operator on Eqn. 1 with respect to time and apply the divergence operator on Eqn. 2. Subtracting the modified continuity equation from the divergence of the momentum equation, then adding the difference of the double divergence of the pressure and the double divergence of the density scaled by the speed of sound to both sides of the resulting equation and simplifying yields Lighthill's [8] acoustic analogy

$$\frac{\partial^2 \rho}{\partial t^2} - c_\infty^2 \frac{\partial^2 \rho}{\partial x_i \partial x_i} = \frac{\partial^2 T_{ij}}{\partial x_i \partial x_j}, \tag{36}$$

where T_{ij} is the Lighthill stress tensor (see Lighthill [8] for details and discussion). The Green's function of Eqn. 36 is governed by

$$\frac{\partial^2 g}{\partial t^2} - c_\infty^2 \frac{\partial^2 g}{\partial x_i \partial x_i} = \delta\left(\boldsymbol{x} - \boldsymbol{y}\right) \delta\left(t - \tau\right), \tag{37}$$

where $g(\boldsymbol{x}; \boldsymbol{y}, t; \tau)$ is the Green's function, $\boldsymbol{x}$ is an observer location, $\boldsymbol{y}$ is a source location, and δ is the Dirac delta function. It can easily be shown that the solution of Eqn. 37 in three-dimensional space is

$$g(\boldsymbol{x}; \boldsymbol{y}, t; \tau) = \frac{\delta\left(t - \tau - |\boldsymbol{x} - \boldsymbol{y}| c_\infty^{-1}\right)}{4\pi |\boldsymbol{x} - \boldsymbol{y}|} \tag{38}$$

and in the frequency domain

$$g\left(\boldsymbol{x}, \boldsymbol{y}, \omega\right) = \frac{\exp\left[-ikr\right]}{4\pi r}, \tag{39}$$

where $\boldsymbol{r}$ is a vector from source to observer. We now can write the closed form solution of Eqn. 36 as the spectral density of far-field pressure using the theory of Green's functions following the approach of Miller [9], but with some important differences. We assume that the observers (from a cross-spectral point of view) are at the same position, that the flight stream Mach number is zero, and that near-field and mid-field terms are negligible in the far-field. The Green's functions that share the same observer but differing source positions within the jet exhaust plume are approximated by a phase change and $g(\boldsymbol{x}; \boldsymbol{y}, \omega)^* = g(\boldsymbol{x}; \boldsymbol{y}, -\omega)$, where superscript $*$ denotes the complex conjugate.

The density is converted to pressure. We arrive at an equation for the spectral density, S, of acoustic pressure in the far-field that is similar to Eqn. 1.11 of Ffowcs Williams [28]

$$\begin{aligned} S(\boldsymbol{x},\omega) = &\int_{-\infty}^{\infty}\int_{-\infty}^{\infty} \frac{r_i r_j r'_l r'_m}{c_\infty^4 r^2 r'^2} g\left(\boldsymbol{x},\boldsymbol{y},\omega\right) g^*\left(\boldsymbol{x},\boldsymbol{y}',\omega\right) \\ &\times \frac{\partial^4}{\partial\tau^4} R_{ijlm}(\boldsymbol{y},\boldsymbol{\eta},\tau) \exp\left[-i\omega\left(\tau + \frac{r}{c_\infty} - \frac{r'}{c_\infty}\right)\right] d\tau d\boldsymbol{\eta} d\boldsymbol{y}, \end{aligned} \tag{40}$$

where the prime denotes an alternate source position. The subscripts i, j, l, and m imply summation from one to three. We have obtained an equation that is a double volumetric integral over the source and an integral over the retarded time. We require a model for the two-point cross-correlation of the Lighthill stress tensor R_{ijlm}. Here, we adopt a simplified form from Miller [9]

$$\begin{aligned} \frac{\partial^4}{\partial\tau^4} R_{ijlm}(\boldsymbol{y},\boldsymbol{\eta},\tau) = &\frac{4A_{ijlm}\overline{u}^4}{\pi^{1/2} l_s^8}\left(3l_s^4 - 12l_s^2(\xi-\overline{u}\tau)^2 + 4(\xi-\overline{u}\tau)^4\right) \\ &\times \exp\left[\frac{-|\xi|}{\overline{u}\tau_s}\right] \exp\left[\frac{-(\xi-\overline{u}\tau)^2}{l_s^2}\right] \exp\left[\frac{-\eta^2}{l_{sy}^2}\right] \exp\left[\frac{-\zeta^2}{l_{sz}^2}\right], \end{aligned} \tag{41}$$

where A_{ijlm} is a coefficient matrix, l is the turbulent length scale in the axial (subscript s) and radial directions (subscript sy and sz), $\overline{u}$ is the axial averaged velocity component, $\boldsymbol{\eta} = \boldsymbol{\eta}(\xi,\eta,\zeta)$ is a vector from source vectors $\boldsymbol{y}$ to $\boldsymbol{y}'$, and τ_s is a turbulent time scale. This model is carefully chosen to both be integratable analytically and capture trends of measurement of turbulent jets in the range of $0.5 \leq M_j \leq 1.5$. Using the proposed model for R_{ijlm}, the integration of τ in Eqn. 40 can be performed. After simplifying we obtain

$$\begin{aligned} S(\boldsymbol{x},\omega) = &\int_{-\infty}^{\infty}\int_{-\infty}^{\infty} \frac{r_i r_j r'_l r'_m}{c_\infty^4 r^2 r'^2} g\left(\boldsymbol{x},\boldsymbol{y},\omega\right) g^*\left(\boldsymbol{x},\boldsymbol{y}',\omega\right) A_{ijlm} \frac{l_s\omega^4}{\overline{u}} \exp\left[\frac{-i\xi\omega}{\overline{u}}\right] \exp\left[\frac{-|\xi|}{\overline{u}\tau_s}\right] \\ &\times \exp\left[\frac{-\eta^2}{l_{sy}^2}\right] \exp\left[\frac{-\zeta^2}{l_{sz}^2}\right] \exp\left[\frac{-l_s^2\omega^2}{4\overline{u}^2}\right] \exp\left[\frac{-i\omega(r-r')}{c_\infty}\right] d\boldsymbol{\eta} d\boldsymbol{y}. \end{aligned} \tag{42}$$

Let us now examine the volumetric integral involving $\boldsymbol{\eta}$. The term $gg^* \exp[-i\omega(r-r')c_\infty^{-1}]$ is approximated as $gg^*(\boldsymbol{y})$, thus removing its dependence on $\boldsymbol{\eta}$ and is removed from the integrand of $\boldsymbol{\eta}$. This approximation is valid as long as $\boldsymbol{x}$ is in the far-field. Using the same far-field argument, we also note that the $r_i r_j r'_l r'_m$ term is no longer dependent on $\boldsymbol{\eta}$. The prime notation can now be dropped. The integrals involving the cross-stream variation can be directly evaluated. The term A_{ijlm} represents coefficients of the fourth order two-point cross-correlation of the stress tensor. We propose a model for A_{ijlm} that is considerably simplified from Miller [9]

$$A_{ijlm} = P_f \sigma^{1/2} A_{ij}^2 S_y, \tag{43}$$

where σ is a function that is dependent on the Mach number and frequency of the acoustic radiation

$$\sigma = \exp\left[-\left(\ln[St] - \ln\left[\frac{7}{100} + \frac{13}{100}(1-M_j)\right]\right)^2 \left(1 + \frac{3}{5}\left(M_j - 1\right)\right)\sigma_f^4\right]. \tag{44}$$

The function σ_f is

$$\sigma_f = \begin{cases} \frac{[(1-M_cM_j)^2+(\beta_sM_cM_j)^2]^{1/2}}{[(1-M_cM_jr_1/r)^2+(\beta_sM_cM_j)^2]^{1/2}} & \text{for } M_cM_j < 1 \\ \frac{\beta_sM_cM_j}{[(1-M_cM_jr_1/r)^2+(\beta_sM_cM_j)^2]^{1/2}} & \text{for } M_cM_j \geq 1. \end{cases} \tag{45}$$

This form is selected to capture fifth power convective amplification effects as proposed by Ffowcs Williams [28]. The first coefficient of A_{ij} is

$$a_{11} = \left\{ \frac{\left[1+(\beta_sM_cM_j)^2\right]^{1/2}}{[(1-M_cM_jr_1/r)^2+(\beta_sM_cM_j)^2]^{1/2}} \right\}^{5/2} \tag{46}$$

and all others are approximately 1/3. The form of the coefficient a_{11} is chosen based on the model of Ffowcs Williams [28], and $\beta_s = 10^{-1}$ is a constant. The convective Mach number coefficient is $M_c = 0.70$. Recall that the convective Mach number, as discussed by Petitjean et al. [3], plays an important role in nonlinear propagation of jet noise. The equivalent spatial source distribution is modeled by the term S_y in Eqn. 43 as

$$S_y = k_{max}^2\overline{\rho}^2 \left(1+\frac{St^{-3}}{200}\right) \exp\left[-\frac{5}{2}\ln\left[\frac{y_1D_jSt^{1/10}}{y_c}\right]^2\right], \tag{47}$$

where $k_{\max}$ is the maximum effective turbulent kinetic energy in the jet plume. Extensive numerical simulations suggest that $k_{\max}$ is approximately

$$k_{max} = k_fM_j^{5/2}\mathrm{TTR}^{Pr+Pr_t\left(1-\mathrm{erf}\left[2M_j^2\right]\right)}, \tag{48}$$

where Erf is the error function, $k_f = 3\times10^3$ is a constant, $Pr = 0.72$ is the Prandtl number, and $Pr_t = 0.90$ is the turbulent Prandtl number. The total temperature ratio (TTR) is the plenum stagnation temperature divided by the ambient static temperature. The axial turbulent length scale is approximated as $l_sD^{-1} = 1.07\left(0.1028M_j+0.0654\right)y_1D_j^{-1}$. The cross-stream turbulent length scales, l_{sy} and l_{sz}, are one-third of l_s. The turbulent time scale is a function of the local turbulent length scale, $\tau_s = l_s\overline{u}^{-1}$. The spatially varying time-averaged stream-wise velocity component and temperature are approximated using the models of Lau et al. [29] and Lau [30]. These are dependent on the jet core length and are estimated using the model of Tam [31]. These models are valid for jets in the range of $0.40 < M_j < 1.5$, but we will be exercising this model well outside its range of validity in the following section. Using these models and assumptions, we simplify the spectral density of pressure in the far-field as

$$\begin{aligned} S(\boldsymbol{x},\omega) = \frac{\pi\omega^4}{c_\infty^4}g\left(\boldsymbol{x},\omega\right)g^*\left(\boldsymbol{x},\omega\right) \int_{-\infty}^{\infty} A_{ijlm}\frac{r_ir_jr_lr_m}{r^4}\frac{l_sl_{sy}l_{sz}}{\overline{u}}\exp\left[\frac{-l_s^2\omega^2}{4\overline{u}^2}\right] \\ \times \int_{-\infty}^{\infty}\exp\left[\frac{-i\xi\omega}{\overline{u}}\right]\exp\left[\frac{-|\xi|}{\overline{u}\tau_s}\right]d\xi dy_1. \end{aligned} \tag{49}$$

Equation 49 is used to make predictions of jet mixing noise in the far-field and is in an important form. It shows that the spectral density from jet mixing noise in the far-field is a volumetric integration that describes a source spectrum that is centered on a point that is approximated at the nozzle exit. Note that the development of Eqn. 49 is considerably more empirical than other approaches, but is beneficial to illustrate the proposed concepts. Equation 39 implies that the term

gg^* in Eqn. 49 is $(16\pi^2 r^2)^{-1}$ and that the energy decays according to spherical spreading. The remaining part of Eqn. 49 defines the jet mixing noise source spectrum. Now, in Eqn. 49 we discount the term gg^* and retain terms that define the source spectrum. In place of gg^*, we use an equivalent expression obtained from the numerical solution of the generalized Burgers' equation. The boundary condition of the numerical implementation of the generalized Burgers' equation is now the broadband source spectrum defined by Eqn. 49. In essence, we have implemented an equivalent form for gg^*. For low amplitude sources (source spectrum), the far-field spectral density predicted using the modified approach is equivalent to that predicted with the more traditional approach. High amplitude sources will cause the nonlinear term within the generalized Burgers' equation to be dominant, and in turn all the characteristics of nonlinear propagation will be apparent in the predicted jet mixing noise spectrum. Furthermore, the effects of atmospheric absorption and dispersion are directly contained in the solution and not accounted for at a later point. Astute readers will note that direct approaches to calculate a Green's function with a Burgers' like equation, such as the collapsing sphere approach, will violate the principle of linear superposition. Also, unlike other approaches to propagate broadband noise that start outside the source region, we propagate the source spectrum from within its source volume of origin.

The implementation of Eqn. 49 is similar to that of Miller [9] but highly simplified due to lack of a second observer. Here, the major difference is the integration of the generalized Burgers' equation and atmospheric effect numerical solvers. The integrals of Eqn. 49 are approximated numerically.

3 Results

The purpose of this section is to show solutions of equations previously developed graphically . First, the Fay (Eqn. 21), Fubini (Eqn. 29), and BBF (Eqn. 33) are evaluated for plane wave propagation. Their respective power spectral density (PSD) is calculated. We then compare solutions of the BBF to measurement data from the Normal Incidence Tube (NIT). Numerical solutions of the generalized Burgers' equation (Eqn. 13) are compared with the BBF (Eqn. 33). The propagation of a jet mixing noise pressure time history is demonstrated with the numerical solver. Finally, example predictions for jet mixing noise far-field spectral density with nonlinear propagation effects are performed using the newly proposed approach.

3.1 Examination of the Fay, Fubini, and Blackstock Bridging Function

We have surveyed mathematically the relation between the Fay (Eqn. 21) and Fubini (Eqn. 29) solutions and the BBF (Eqn. 33) with governing equations. Here, we will illustrate their physical significance graphically. Figure 1 shows the amplitudes of the three solutions as a function of non-dimensional distance from a sinusoidal boundary condition. The contribution of Fay (Eqn. 21) is shown as a dashed line with squares, the contribution of Fubini (Eqn. 29) is shown as a dash-dot line with triangles, and the BBF (Eqn. 33) is shown as a solid line. The amplitudes are normalized with respect to the amplitude of the source at $\sigma = 0$. Recall that $\sigma = x\overline{x}^{-1}$. The amplitude is calculated numerically by summing the Fourier coefficient magnitudes over all frequencies at each spatial position. Due to the assumptions and method of solution of Fubini (Eqn. 29), the Fubini solution is valid from $0 \leq \sigma < 1$. It immediately decays and approaches zero as the limit $\sigma \to \infty$. Fay, who sought stable waveforms, shows a valid solution for $\sigma > 3.5$ until viscous effects dominate the dynamics of wave propagation. Within the region $1 \leq \sigma < 3.5$ neither the Fay or Fubini solution are correct. The BBF bridges the two solutions and satisfies (at least to engineering accuracy) the generalized Burger's equation.

We now examine the waveform of the BBF at various propagation distances. At the boundary condition ($\sigma = 0$) the solution is known and is illustrated in Fig. 2. For example purposes we select a frequency of 3000 Hz and an initial pressure amplitude of $p_o = 496.07$ Pa, which is 144.88 dB. The resultant wavenumber is 54.96 m^{-1}. Ambient conditions are specified as $\rho_\infty = 1.213$ kg m^{-3}, $c_\infty = 343$ m s^{-1}, and $\beta = 1.2$. Based on this boundary condition the shock formation distance is $\overline{x} = 4.362$ m. The initial waveform, shown as a function of observer time, is presented in Fig. 2(a). The PSD of the periodic boundary condition is shown in Fig. 2(b). Unsurprisingly, the PSD contains only one non-zero discrete component.

The BBF is now evaluated at $\sigma = 1$, the shock formation location, and $\sigma = 5.73$, which is well within the validity of the Fay solution. The boundary condition remains the same. These waveforms are shown in Figs. 3(a) and 4(a). After the waveform is 'shocked' there are many non-zero components in the PSD, as shown in Figs. 3(b) and 4(b).

These solutions are well known to acousticians well versed in the theory of finite amplitude waves, however this review is conducted to illustrate important points relative to acoustic analogy theory. Unlike infinitesimal acoustics, multiple non-zero frequency domain Fourier components appear that are non-negligible that are due to propagation effects. Furthermore, the Gibbs phenomenon appears when we restrict our mathematics to finite numerical approximations. Due to these nonlinearities we are unable to use the principle of superposition that is central to the evaluation of an acoustic analogy with a volumetric source.

3.2 Comparison of the Blackstock Bridging Function with Measurement Data of the Normal Incidence Tube

Measurement data of weakly nonlinear propagating plane waves is obtained from the NIT of NASA Langley Research Center. Schultz et al. [32] discussed the NIT as part of a larger investigation. The NIT is shown in Fig. 5(a). Six speakers are driven by a function generator and create plane waves at specific frequencies and amplitudes. These carefully constructed waves propagate down the circular tube and impinge on a liner sample. Normally, the NIT is used to measure the normal incidence of various materials for use in aircraft engine liners. Here, a liner is selected that effectively absorbs the entire wave thereby eliminating reflection. This liner would not normally be placed in a flight vehicle because of its size and bulk. Figure 5(b) shows a simplified flow chart that describes the operation of the NIT. A function generator creates a signal that is amplified and subsequently drives the speaker array. The microphone signals are conditioned and captured with a digital computer. These signals are then analyzed using digital spectral analysis. High pass filters are utilized with cut-offs below the planar wave excitation frequency. A microphone is located near the top of the NIT to measure the source and multiple 'measurement' microphones reside near the liner. The reference and measurement microphones are used to capture near sinusoidal plane waves for validation purposes.

We evaluate the BBF (Eqn. 33) and compare solutions with various measurements from the NIT. Figure 6 shows three examples of these comparisons that are representative of a larger investigation. The BBF is shown as a solid line and the measurement is shown as a dashed-dotted line. Three comparisons are shown for 140.03 dB at 3000 Hz, 147.94 dB at 2000 Hz, and 144.88 dB at 3000 Hz, in Figs. 6(a), 6(b), and 6(c) respectively. Note the y-axis represents pressure in Pascal and the x-axis represents retarded time. Generally, this theory and measurement are in agreement both in magnitude and phase. The relatively short propagation distance within the NIT only allows for waveforms that are minimally distorted by nonlinear propagation. This is not a major problem because our focus is on jet mixing noise sources that are approximately 165 dB, that is near the limit of weak shock theory. Based on these validations, we believe that the implementation of the

BBF is correct. There is no reason to expect that larger propagation distances will deviate from these results.

3.3 Comparison of the Numerical Propagation Solver with the Blackstock Bridging Function

We have some confidence that the BBF is evaluated correctly using a numerical technique. We attempt to gain additional confidence in the solution strategy of the generalized Burgers' equation by making extensive comparisons with numerical solutions of the BBF. Table 1 summarizes the conditions examined. At the source position, $\sigma = 0$, the boundary condition $p(0,t) = p_o \sin[2\pi f t]$ is applied. Four values of p_o are chosen, 2.82843 Pa, 89.4427 Pa, 282.843 Pa, and 2828.43 Pa, that result in tonal sound pressure level (SPL) of 100 dB, 130 dB, 140 dB, and 160 dB respectively. At each SPL a frequency of 100 Hz, 1 kHz, 10 kHz, and 100 kHz are applied. For each combination of frequency and wave amplitude, the planar shock formation distance is calculated using Eqn. 23. Numerical solutions of plane wave propagation are calculated at three non-dimensional positions, halfway to shock formation, $\sigma = 1/2$, at the shock formation, $\sigma = 1$, and three times the shock formation, $\sigma = 3$. Comparisons of these numerical solutions are shown in Figure 7. In each subfigure the y-axis is pressure in Pascal and the x-axis is retarded time, τ, in seconds. These figures are a sampling of a larger validation database and are representative of all results. Figures 7(a) and 7(b) have a boundary condition of 130 dB at 100 Hz and 1000 Hz. Note that the shock formation distances at the lower frequencies in Figs. 7(a), 7(c), and 7(e) are much larger than the higher frequencies of Figs. 7(b), 7(d), and 7(f). The numerical solution in the pre-shock region ($\sigma < 1$) agrees very well with the BBF in magnitude and phase. In the post shock region ($\sigma > 1$) the Gibbs phenomenon is apparent. This can be minimized or even almost entirely eliminated by increasing the number non-zero Fourier coefficients, but doing so increases the amount of computer memory used by the numerical solver significantly. Unfortunately, in some cases numerical error accumulates for boundary conditions that are very high in amplitude and frequency. For example, in Fig. 7(f) near $\tau \approx 5 \times 10^{-5}$ s and $\sigma = 3$, small oscillations occur in an 'odd function fashion,' centered about zero. Extensive numerical evaluations using the developed approach have shown that these spurious oscillations do not grow significantly except at extremely large distances. Overall, the agreement between the developed numerical method for the evaluation of the generalized Burgers' equation more than satisfactorily captures the trends of nonlinear propagation of tonal sources.

3.4 Propagation of a Broadband Spectrum

The developed mathematical approach requires that the source spectrum propagate from its location of origin to observer in the far-field. Here, we propagate a measured broadband jet noise spectrum from the near-field to the far-field to demonstrate the approach. Note that the phase of each wavenumber component is unknown if only a power spectrum is available from measurement. A random phase is assigned to each of the frequency components of the measured signal. This is an important point as the developed prediction method is for spectral density and does not contain phase. A high speed heated jet at $M_j = 1.86$ and TTR = 3.20 produces a waveform at the side line location of one hundred nozzle diameters ($R/D = 100$). The measured (source) and propagated (observer) spectrum are shown in Fig. 8(a), where 'measured' represents the processed spectrum at $R/D = 100$. The propagated spectrum, found by numerical solution of the generalized Burgers' equation (Eqn. 9), is also shown in Fig. 8(a) as the solid line with circles. The observer spectrum is at $R/D = 200$, twice the distance of the measurement location relative to the source. At low through mid frequencies a decrease of $20 \log_{10}[2] \approx 6.02$ dB of sound power is predicted. This is

consistent with the theory of linear acoustics. At high frequencies, simple spherical spreading is not apparent and only approximately four dB of reduction in SPL is predicted. This is due to the nonlinear term dominating atmospheric absorption and the transition of energy from lower wavenumbers to higher wavenumbers. At low through mid frequencies, the same fine 'peaks' and 'troughs' are present in the spectrum at both field locations. These features are highly distorted between field locations at high frequencies due to nonlinear propagation effects, atmospheric absorption (dissipation and dispersion), and energy transfer. At very high frequencies additional energy is present due to the Gibbs phenomenon.

The time history of the spectrum can be compared with the use of the inverse Fourier transform. The pressure time histories of these spectra are shown in Fig. 8(b), where the y-axis is the pressure in Pascal and the x-axis represents time. Note that the observer time is not equal to the measured time, and the propagated signal is translated by $t - \tau$ for the purpose of directly comparing the waveform distortion. Observe wave steepening near certain measured time signals such as $t \approx 0.608$ s or 0.6108 s. Figure 8(c) shows the details of the wave coalescence of one particular portion of the pressure time history. At these times among many, the waves have coalesced into a shock that exhibits a significant amount of overpressure. Lower amplitude waves, for example near $t \approx 0.6075$ s, have only lost energy and not coalesced into a discontinuity. Waves with less energy are dominated locally through the mechanisms of spherical spreading and atmospheric absorption, that are more dominant than the nonlinear mechanisms present with the generalized Burgers' equation. We offer no further validation of this numerical approach because it is widely used by many investigators (see for example Saxena et al. [17] or McInerny et al. [6]) to propagate both rocket and jet noise.

3.5 Example Predictions of Jet Mixing Noise Including Nonlinear Propagation Effects

Now, the numerical method for the solution of the generalized Burgers' equation with almost no alteration will be combined with the source spectrum predicted with an acoustic analogy. Figure 9 shows example predictions from the newly developed approach. The jet operates at $M_j = 1.86$ and TTR = 3.20. Observers are located in the sideline direction of the jet at radial locations $R/D = 100$, 140, 200, 240, and 300. The y-axis is SPL per unit St and the x-axis is Strouhal number, and the former values have been normalized by u_j and D_j. The solid line represents the prediction using the newly developed approach at $R/D = 100$. This component of jet noise can be interpreted as the contribution from the relatively incoherent turbulence. Other predictions that include nonlinear propagation effects are variations of dashed lines and are labeled in the legend of Fig. 9. These predictions are based on the source spectrum defined by Eqn. 49. To assess the effects of nonlinear propagation relative to linear propagation, predictions using spherical spreading and atmospheric absorption of Bass et al. [21,22] are shown in Fig. 9 as symbols. These linear acoustic predictions are located at the propagation distance $R/D = 100$. For example, at $R/D = 200$, the dash-dot-dash line is the prediction from the jet mixing noise propagated nonlinearly from the source, and the triangles represent linear propagation using spherical spreading and atmospheric absorption from the $R/D = 100$ prediction. Like the previous example shown for purely broadband noise propagation, we observe a rise in high frequency energy and a generally consistent spherical spreading rate at low and mid frequencies. Note that the peak SPL per unit St at $R/D = 100$ is approximately 164 dB at $St \approx 0.25$, that is considerably energetic. Numerical experiments with this method with less intense acoustic radiation show traditional linear acoustic spreading and atmospheric absorption, that is generally observed in almost all commercial jet noise measurements and predictions. At high frequencies some of the energy is due to the Gibbs phenomenon. This fictitious additional energy can be eliminated by including more non-zero harmonic components in

the nonlinear propagation solver. Furthermore, these results are based upon a source model that is developed for jet Mach numbers up to approximately 1.50, and the overall levels and scaling might be misleading. To validate and refine this theory, a comprehensive experimental database of high speed on-design jets must be created, with multiple observer points at various field positions. It is hopeful that in the future such a database will be available to validate this newly developed theory.

4 Conclusion

An acoustic analogy is proposed that takes into account nonlinear propagation effects from the source to observer. Propagation effects are captured by approximating the modulus squared of the Green's function of the wave equation with a numerical solution in a form of the generalized Burgers' equation. The numerical solution of the generalized Burgers' equation is validated with the use of the Blackstock bridging function and measurement data, that are in turn validated with the Fay and Fubini solutions. A mathematical survey of the connection between the acoustic analogy and equations governing propagation is shown based upon the Navier-Stokes equations. The source model and approximation of the propagation mechanism are consistent with the governing equations. An example of the method based on simplified source models and the nonlinear propagation numerical algorithm is shown for a high intensity on-design jet.

Validation data is limited for high intensity on-design jets. To fully validate and refine this theory, a comprehensive experimental database of high speed on-design jet noise must be created, with various field positions. This data would facilitate the creation of a more advanced source model for the sound from compressible jet turbulence and help improve the connection between the turbulent source and nonlinear propagation algorithms. It is hopeful that such a database will become available to validate this newly developed theory.

References

1. Neilsen, T. B., Gee, K. L., and James, M. M., "Spectral Characterization in the Near and Mid-Field of Military Jet Aircraft Noise," *19th AIAA/CEAS Aeroacoustics Conference, AIAA Paper 2013-2191*, 2013. doi:10.2514/6.2013-2191.

2. Gee, K. L., Shepherd, M. R., Falco, L. E., Atchley, A. A., Ukeiley, L. S., Jansen, B. J., and Seiner, J. M., "Identification of Nonlinear and Near-Field Effects in Jet Noise using Nonlinearity Indicators," *13th AIAA/CEAS Aeroacoustics Conference, AIAA Paper 2007-3653*, 2007. doi:10.2514/6.2007-3653.

3. Petitjean, B., Viswanathan, K., and McLaughlin, D. K., "Acoustic Pressure Waveforms Measured in High Speed Jet Noise Experiencing Nonlinear Propagation," *International Journal of Aeroacoustics*, Vol. 5, No. 2, 2006, pp. 193–215. doi:10.1260/147547206777629835.

4. Tam, C. K. W. and Parrish, S. A., "Noise of High-Performance Aircrafts at Afterburner," *20th AIAA/CEAS Aeroacoustics Conference, AIAA Paper 2014-2754*, 2014. doi:10.2514/6.2014-2754.

5. Morfey, C. L. and Howell, G. P., "Nonlinear Propagation of Aircraft Noise in the Atmosphere," *AIAA Journal*, Vol. 19, No. 8, 1980, pp. 986–992. doi:10.2514/3.51026.

6. McInerny, S. A. and Olcmen, S. M., "High-Intensity Rocket Noise: Nonlinear Propagation, Atmospheric Absorption, and Characterization," *Journal of the Acoustical Society of America*, Vol. 117, No. 2, 2005, pp. 578–591. doi:10.1121/1.1841711.

7. Gee, K. L., Giraud, J. H., Blotter, J. D., and Sommerfeldt, S. D., "Energy-Based Acoustical Measurements of Rocket Noise," *15th AIAA/CEAS Aeroacoustics Conference, AIAA Paper 2009-3165*, 2009. doi:10.2514/6.2009-3165.

8. Lighthill, M. J., "On Sound Generated Aerodynamically. I. General Theory," *Proc. R. Soc. Lond. A.*, Vol. 211, No. 1107, 1952, pp. 564–587. doi:10.1098/rspa.1952.0060.

9. Miller, S. A. E., "Prediction of Near-Field Jet Cross Spectra," *AIAA Journal*, 2015. doi:10.2514/1.J053614.

10. Schlichting, H. and Gersten, K., "Boundary-Layer Theory," *Springer-Verlag, New York*, 2000.

11. Crighton, D. G., "Model Equations of Nonlinear Acoustics," *Annual Review of Fluid Mechanics*, Vol. 11, 1979, pp. 11–33. doi:10.1146/annurev.fl.11.010179.000303.

12. Blackstock, D. T., "Generalized Burgers Equation for Plane Waves," *Journal of the Acoustical Society of America*, Vol. 77, No. 6, 1985, pp. 2050–2053. doi:10.1121/1.391778.

13. Blackstock, D. T., "History of Nonlinear Acoustics and a Survey of Burgers and Related Equations," *Proceedings of a Conference held at the Applied Research Laboratories, The University of Texas at Austin*, 1969, pp. 1–27.

14. Vladimirov, V. A. and Maczka, C., "Exact Solutions of Generalized Burgers Equation, Describing Travelling Fronts and Their Interaction," *Reports on Mathematical Physics*, Vol. 60, No. 2, 2007, pp. 317–328. doi:10.1016/S0034-4877(07)80142-X.

15. Mendousse, J. S., "Nonlinear Dissipative Distortion of Progressive Sound Waves at Moderate Amplitudes," *Journal of the Acoustical Society of America*, Vol. 25, No. 51, 1953, pp. 51–54. doi:10.1121/1.1907007.

16. Lighthill, M. J., "Viscosity Effects in Sound Waves of Finite Amplitude," *Surveys in Mechanics, Cambridge University Press (Davies R. M. and Batchelor, G. K. (Eds.))*, 1956, pp. 250–351.

17. Saxena, S., Morris, P. J., and Viswanathan, K., "Algorithm for the Nonlinear Propagation of Broadband Jet Noise," *AIAA Journal*, Vol. 47, No. 186-194, 2009, pp. 186–194. doi:10.2514/1.38122.

18. Lee, S. L., Morris, P. J., and Brentner, K. S., "Improved Algorithm for Nonlinear Sound Propagation with Aircraft and Helicopter Noise Applications," *AIAA Journal*, Vol. 48, No. 11, 2010, pp. 2586–2595. doi:10.2514/1.J050396.

19. Saxena, S., "A New Algorithm for Nonlinear Propagation of Broadband Jet Noise," *M.S. Thesis, The Pennsylvania State University*, 2008.

20. Duchon, C. E., "Lanczos Filtering in One and Two Dimensions," *Journal of Applied Meteorology*, Vol. 18, No. 8, 1979, pp. 1016–1022.

21. Bass, H. E., Sutherland, L. C., Zuckerwar, A. J., Blackstock, T. D., and Hester, D. M., "Atmospheric Absorption of Sound: Further Developments," *Journal of the Acoustical Society of America*, Vol. 97, No. 1, 1995, pp. 680–683. doi:10.1121/1.412989.

22. Bass, H. E., Sutherland, L. C., Zuckerwar, A. J., Blackstock, T. D., and Hester, D. M., "Erratum: Atmospheric Absorption of Sound: Further Developments," *Journal of the Acoustical Society of America*, Vol. 99, No. 2, 1995, pp. 1259–1259. doi:10.1121/1.415223.

23. Fay, R. D., "Plane Sound Waves of Finite Amplitude," *Journal of the Acoustical Society of America*, Vol. 3, No. 9, 1931, pp. 222–241. doi:10.1121/1.1901928.

24. Blackstock, D. T., "Connection Between the Fay and Fubini Solutions for Plane Sound Waves of Finite Amplitude," *Journal of the Acoustical Society of America*, Vol. 39, No. 6, 1965, pp. 1019–1026. doi:10.1121/1.1909986.

25. Fubini-Ghiron, E., "Anomalie nella Propagazione di onde Acustiche di Grande Ampiezza," *Alta Frequenza*, Vol. 4, 1935, pp. 530–581.

26. Westervelt, P. J., "The Mean Pressure and Velocity in a Plane Acoustic Wave in a Gas," *The Journal of the Acoustical Society of America*, Vol. 22, No. 3, 1950, pp. 319–327. doi:10.1121/1.1906606.

27. Earnshaw, S., "On the Mathematical Theory of Sound," *Phil. Trans. R. Soc. London*, Vol. 150, 1860, pp. 133–148. doi:10.1098/rstl.1860.0009.

28. Ffowcs Williams, J. E., "The Noise from Turbulence Convected at High Speed," *Phil. Trans. R. Soc. Lond. A*, Vol. 255, No. 1063, 1963, pp. 469–503. doi:10.1098/rsta.1963.0010.

29. Lau, J. C., Morris, P. J., and Fisher, M. J., "Measurements in Subsonic and Supersonic Free Jets using a Laser Velocimeter," *Journal of Fluid Mechanics*, Vol. 93, No. 1, 1979, pp. 1–27. doi:10.1017/S0022112079001750.

30. Lau, J. C., Morris, P. J., and Fisher, M. J., "Effects of Exit Mach Number and Temperature on Mean-Flow and Turbulence Characteristics in Round Jets," *Journal of Fluid Mechanics*, Vol. 105, No. 1, 1981, pp. 193–218. doi:10.1017/S0022112081003170.

31. Tam, C. K. W., "Broadband Shock-Associated Noise of Moderately Imperfectly Expanded Jets," *Journal of Sound and Vibration*, Vol. 140, No. 1, 1990, pp. 55–71. doi:10.1016/0022-460X(90)90906-G.

32. Schultz, T., Liu, F., Cattafesta, L., Sheplak, M., and Jones, M., "A Comparison Study of Normal-Incidence Acoustic Impedance Measurements of a Perforate Liner," *15th AIAA/CEAS Aeroacoustics Conference, AIAA Paper 2009-3301*, 2009. doi:10.2514/6.2009-3301.

Table 1. Validation cases for the numerical propagation algorithm.

p_o (Pa)	dB	f (kHz)	Shock Distance (m)	σ_1	σ_2	σ_2
2.82843	100	0.10	22801.5	0.5	1	3
2.82843	100	1.00	2280.15	0.5	1	3
2.82843	100	10.0	228.015	0.5	1	3
2.82843	100	100	22.802	0.5	1	3
89.4427	130	0.10	721.047	0.5	1	3
89.4427	130	1.00	72.105	0.5	1	3
89.4427	130	10.0	7.210	0.5	1	3
89.4427	130	100	0.721	0.5	1	3
282.843	140	0.10	228.015	0.5	1	3
282.843	140	1.00	22.802	0.5	1	3
282.843	140	10.0	2.280	0.5	1	3
282.843	140	100	0.228	0.5	1	3
2828.43	160	0.10	22.802	0.5	1	3
2828.43	160	1.00	2.280	0.5	1	3
2828.43	160	10.0	0.228	0.5	1	3
2828.43	160	100	0.023	0.5	1	3

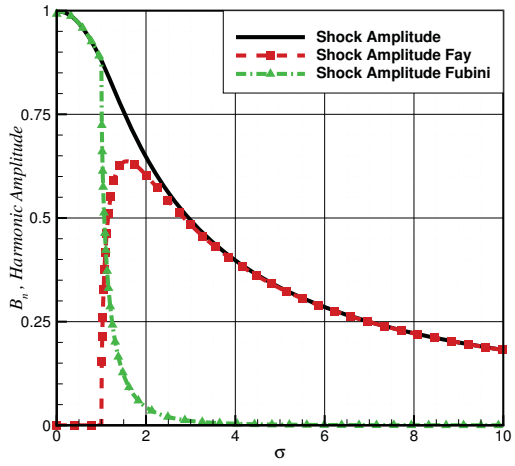

Figure 1. Comparison of harmonic amplitudes of the Fay [23], Fubini [25], and Blackstock [24] bridging function relative to normalized propagation distance.

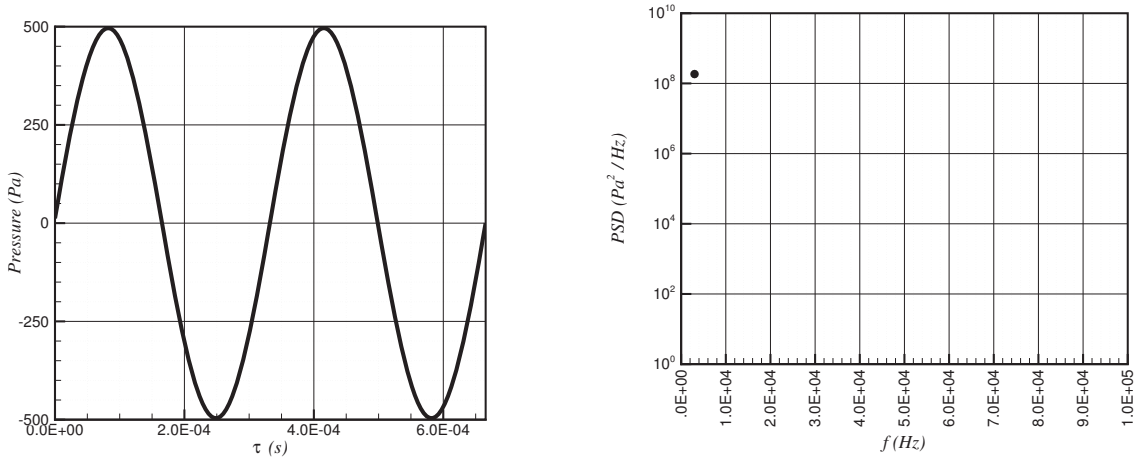

(a) Time history

(b) Power spectral density

Figure 2. Blackstock bridging function at propagation distance $\sigma = 0$.

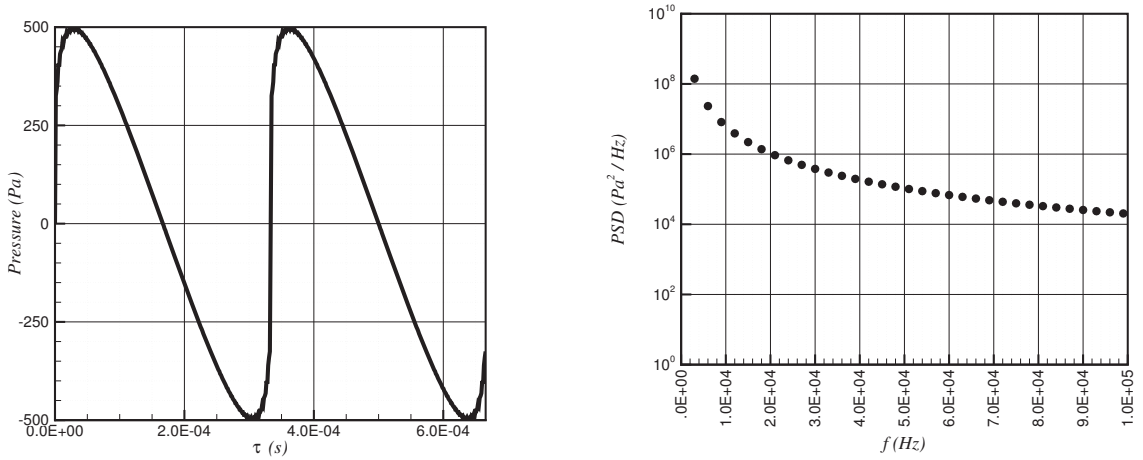

(a) Time history

(b) Power spectral density

Figure 3. Blackstock bridging function at propagation distance $\sigma = 1$.

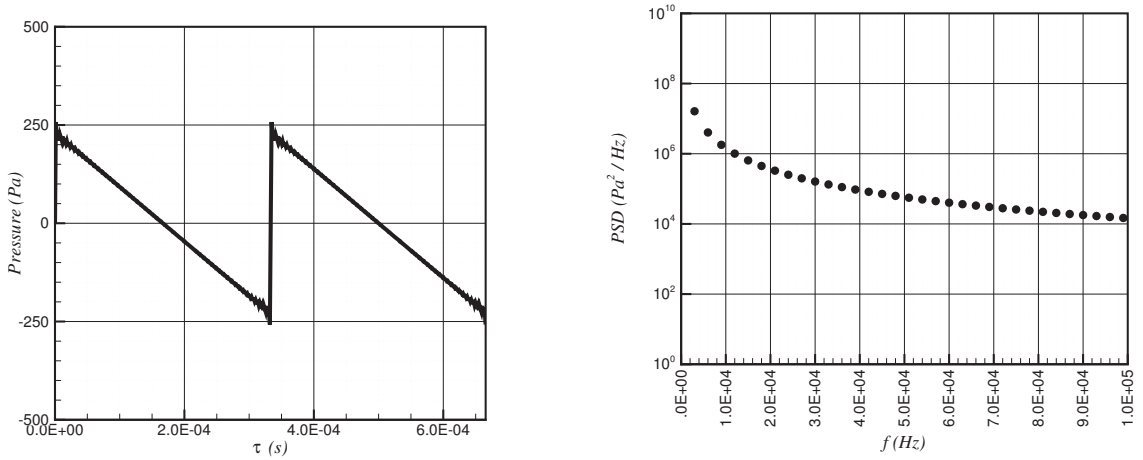

(a) Time history

(b) Power spectral density

Figure 4. Blackstock bridging function at propagation distance $\sigma = 5.73$.

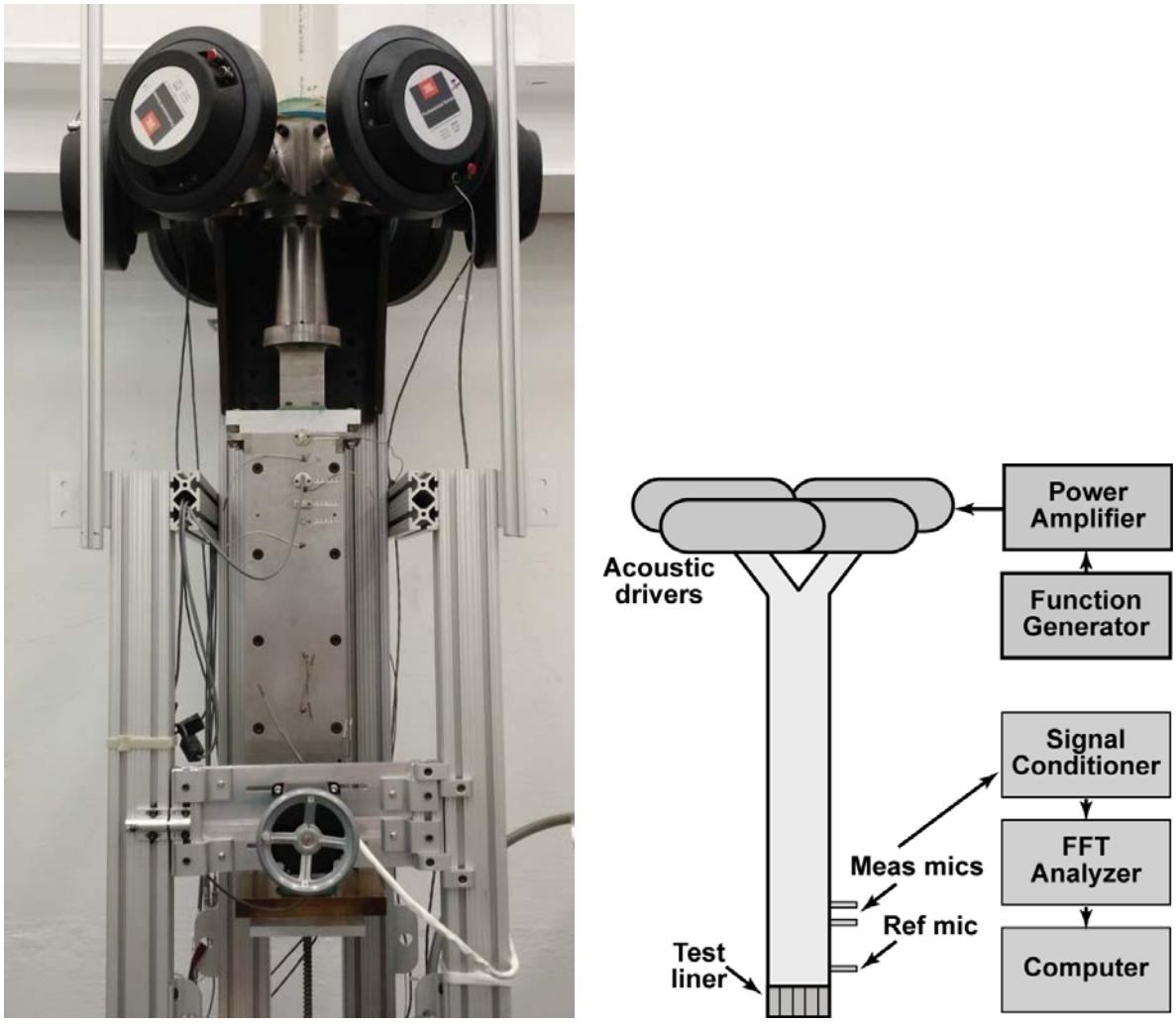

(a) (b)

Figure 5. a) Photograph and b) diagram of the Normal Incidence Tube. Courtesy of Brian Howerton of NASA Langley Research Center.

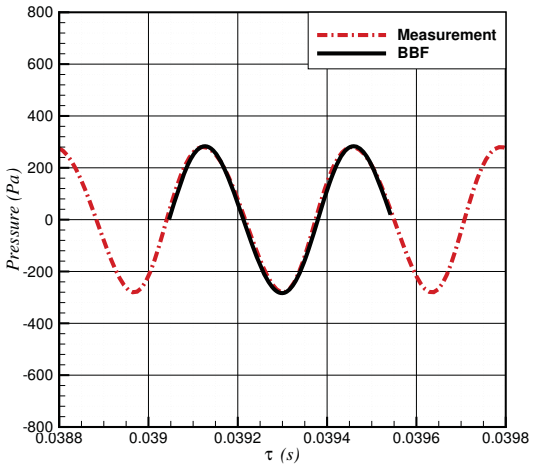

(a) 140.03 dB and 3000 Hz

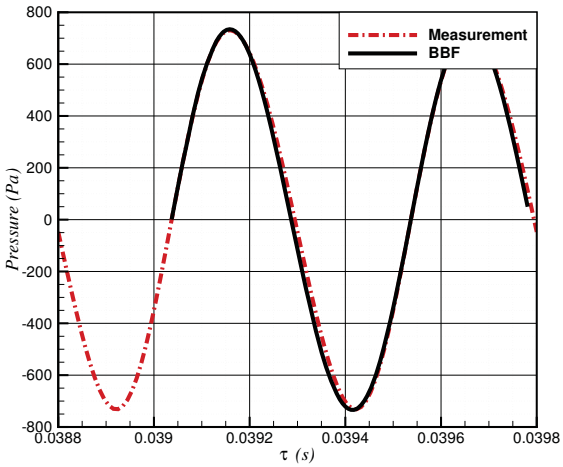

(b) 147.94 dB and 2000 Hz

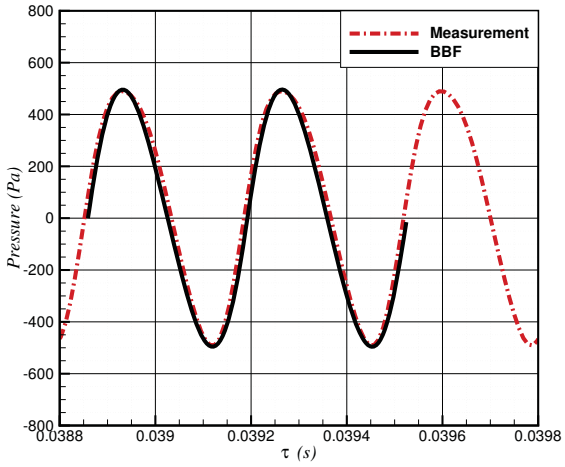

(c) 144.88 dB and 3000 Hz

Figure 6. Comparisons between the Blackstock bridging function and measurement.

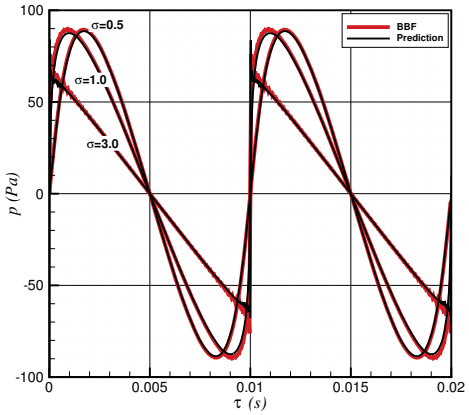

(a) 130 dB and 100 Hz

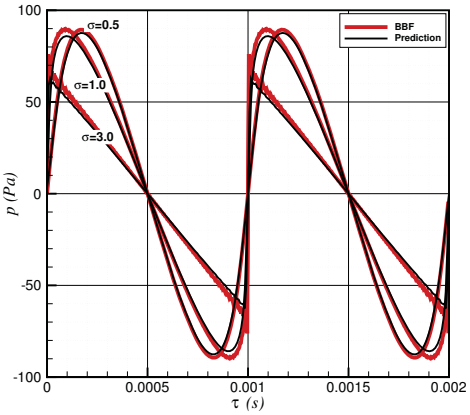

(b) 130 dB and 1000 Hz

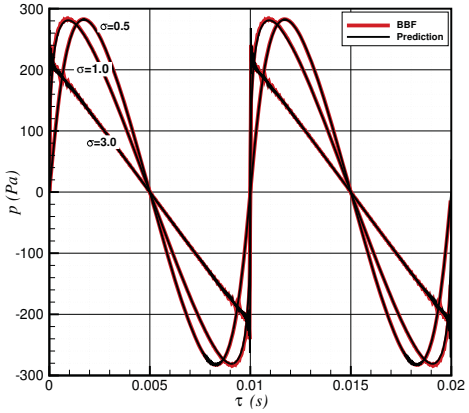

(c) 140 dB and 100 Hz

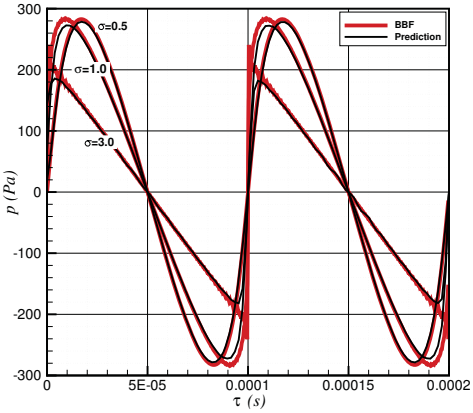

(d) 140 dB and 10000 Hz

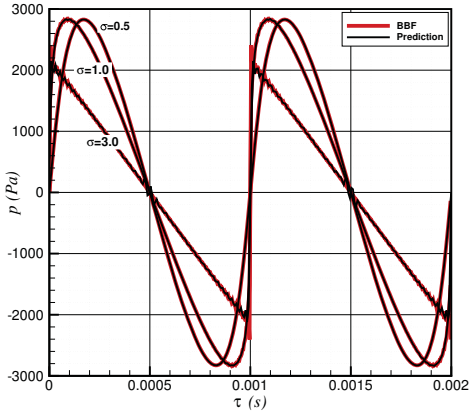

(e) 160 dB and 1000 Hz

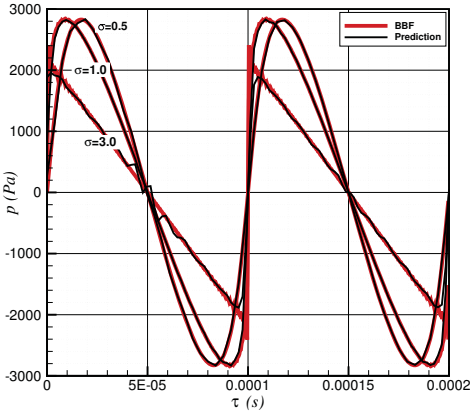

(f) 160 dB and 10000 Hz

Figure 7. Comparisons of the numerical solution of the generalized Burgers' equation with the Blackstock bridging function at various propagation distances σ.

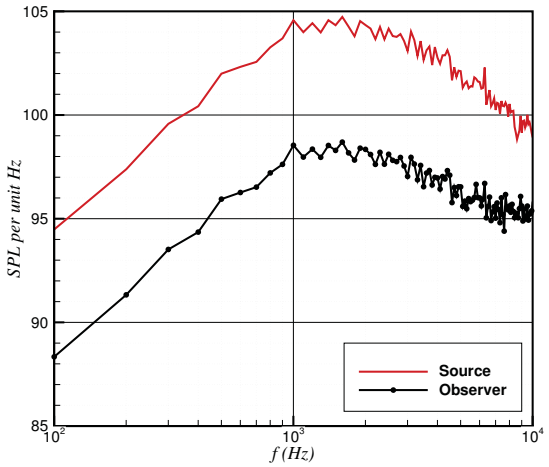

(a) Sound pressure spectrum

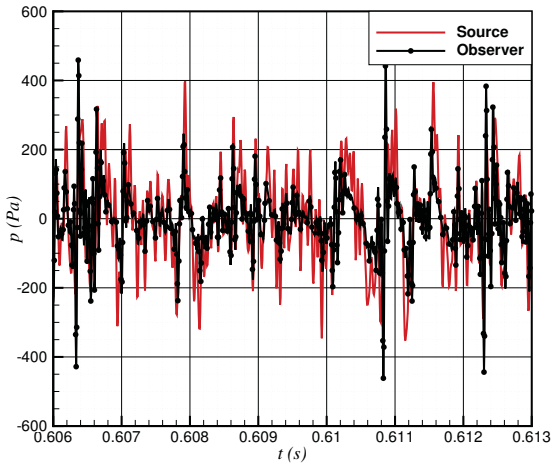

(b) Pressure time history

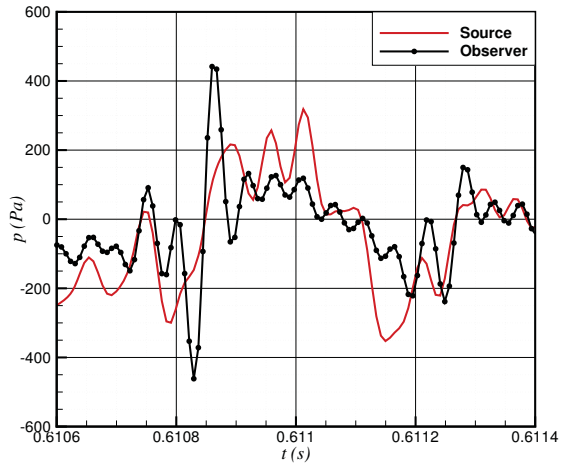

(c) Example of wave coalescence within pressure time history

Figure 8. Example propagation of broadband jet noise in the sideline direction.

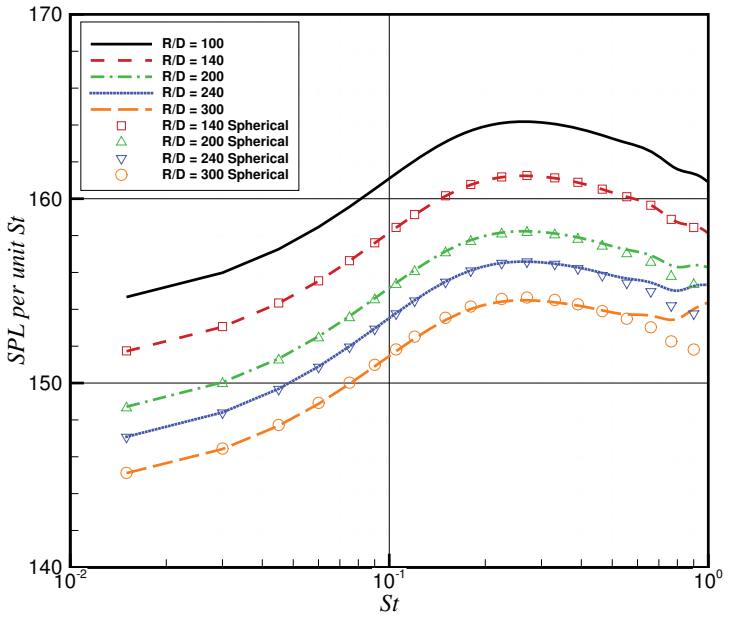

Figure 9. Predictions of jet mixing noise at the sideline direction at various propagation distances.

REPORT DOCUMENTATION PAGE

Form Approved
OMB No. 0704-0188

1. REPORT DATE *(DD-MM-YYYY)*	2. REPORT TYPE	3. DATES COVERED *(From - To)*
01- 04 - 2015	Technical Memorandum	

4. TITLE AND SUBTITLE

Toward a Nonlinear Acoustic Analogy: Turbulence as a Source of Sound and Nonlinear Propagation

5a. CONTRACT NUMBER

5b. GRANT NUMBER

5c. PROGRAM ELEMENT NUMBER

6. AUTHOR(S)

Miller, Steven A. E.

5d. PROJECT NUMBER

5e. TASK NUMBER

5f. WORK UNIT NUMBER

110076.02.07.04.01

7. PERFORMING ORGANIZATION NAME(S) AND ADDRESS(ES)

NASA Langley Research Center
Hampton, VA 23681-2199

8. PERFORMING ORGANIZATION REPORT NUMBER

L-20532

9. SPONSORING/MONITORING AGENCY NAME(S) AND ADDRESS(ES)

National Aeronautics and Space Administration
Washington, DC 20546-0001

10. SPONSOR/MONITOR'S ACRONYM(S)

NASA

11. SPONSOR/MONITOR'S REPORT NUMBER(S)

NASA-TM-2015-218706

12. DISTRIBUTION/AVAILABILITY STATEMENT

Unclassified - Unlimited
Subject Category 71
Availability: NASA STI Program (757) 864-9658

13. SUPPLEMENTARY NOTES

14. ABSTRACT

An acoustic analogy is proposed that directly includes nonlinear propagation effects. Here, we examine the Lighthill acoustic analogy and replace the Green's function of the wave equation with numerical solutions of the generalized Burgers' equation. This is justified mathematically by using similar arguments that are the basis of the solution of the Lighthill acoustic analogy. This approach is superior to alternatives because propagation is accounted for directly from the source to the far-field observer instead of from an arbitrary intermediate point. Validation of a numerical solver for the generalized Burgers' equation is performed by comparing solutions with the Blackstock bridging function and measurement data. Most importantly, the mathematical relationship between the Navier-Stokes equations, the acoustic analogy that describes the source, and canonical nonlinear propagation equations is shown. Finally, example predictions are presented for nonlinear propagation of jet mixing noise at the sideline angle.

15. SUBJECT TERMS

Acoustic analogy; Blackstock; Fay; Fubini; Green's function; Jet; Nonlinear; Propagation; Rocket; Turbulence

16. SECURITY CLASSIFICATION OF:			17. LIMITATION OF ABSTRACT	18. NUMBER OF PAGES	19a. NAME OF RESPONSIBLE PERSON
a. REPORT	b. ABSTRACT	c. THIS PAGE			STI Help Desk (email: help@sti.nasa.gov)
					19b. TELEPHONE NUMBER *(Include area code)*
U	U	U	UU	32	(757) 864-9658